Optical and Quantum Electronics (2022) 54:372
https://doi.org/10.1007/s11082-022-03780-y

Study of structural, electronic, elastic, optical and thermoelectric properties of half-Heusler compound RbScSn: A TB-mBJ DFT study

Besbes Anissa[1] · Djelti Radouan[2] · I. Kars Durukan[3]

Received: 22 January 2022 / Accepted: 28 April 2022 / Published online: 22 May 2022

Abstract
We report the structural, electronic, optical and thermoelectric properties of half-Heusler compound RbScSn within density functional theory (DFT) as implemented in Wien2k and semi-classical Boltzmann transport theory. The Tran-Blaha modified Becke-Johnson (TB-mBJ) potential is adopted to compute accurately the band gap of compound. The optimized lattice constant, bulk modulus and its pressure derivative within GGA and TB-mBJ approaches are reported. For both approximations, the alloy is found to be nonmagnetic semiconductor. Compared to the GGA approach, the TB-mBJ approximation has significantly improved the Gap value by a rate approaching 100%. Electronic calculations show that the RbScSn half-Heusler is an indirect bandgap semiconductor. The computation for elastic constants and mechanical parameters are done to check the mechanical stability, which revealed that the RbScSn is stable with ductile nature and low rigidity. The optical properties such as real and imaginary part of dielectric function, reflectivity, absorption coefficient and refractive index show interesting results. The high absorption coefficient of $11{,}382 \times 10^4$ cm^{-1}, registered at ultraviolet region accompanied by a high reflectivity of 64% observed in near infrared region, indicates the high potential of RbScSn compound to optical applications. Due to the narrow band gap semiconducting nature, the thermoelectric parameters are also calculated. A high merit factor close to unity was registered at room temperature. Based on the obtained results we can predicted that the RbScSn semiconductor is well suitable for some optical and thermoelectric applications.

Keywords Cubic half-Heusler · Semiconductor · Phonon dispersion · Elastic constants · Absorption coefficient · Reflectivity · Merit factor

✉ Djelti Radouan
Radouane.djelti@univ-mosta.dz; djeltired@yahoo.fr

[1] SEA2M Laboratory, University of Mostaganem (UMAB), Mostaganem, Algeria

[2] Technology and Solids Properties Laboratory, University of Mostaganem (UMAB), Mostaganem, Algeria

[3] Department of Physics, Faculty of Science, Gazi University, 06500 Ankara, Turkey

1 Introduction

To address the current energy crisis, in recent years we have seen a dizzying increase in research work on clean energy, energy that produces negligible amounts of waste and pollutants. In order to meet to these requirements, it was necessary to find new materials without carbon, i.e. do not come from fossil sources and that emits little or no CO_2, does not participate or contributes little to the greenhouse effect (Chen and Ren 2013) or to the destruction of the ozone layer. The technology of converting thermal energy into electrical energy through thermoelectric devices (TE) based on innovative materials is proving to be the right solution to this global energy crisis. A best energy conversion performance requires a compound, which exhibit a high merit factor value approaching ~ 1. This criterion can be found in materials that have a narrow band gap and high DOS near the Fermi level (Kaur et al. 2018). Otherwise, an adequate doping can be suggested as a means in order to change the band structure around the Fermi level and thus increase transport performance of materials. Recently, several types of materials have been found adequate for the energy conversion operation, let us quote by way of example the half-Heusler (Bos and Downie 2014; Zhu et al. 2015; Huang et al. 2016), Perovskite (Acharya et al. 2021; Rahman et al. 2022; Sun et al. 2021), skutterudites (Jianga et al. 2022; Rogl et al. 2019; Khan et al. 2017). The material studied in the present research is a half-Heusler (HH) which is a ternary intermetallic compounds with the general formula ABC, where B is a highly electronegative transition metal. A is a weakly electronegative transition metal or alkaline element and C is the main group element (Amiri et al. 2022; Hoat et al. 2020; Shakil et al. 2019). The HH crystal structure consists of three interpenetrating ordered fcc sublattices. During these last years, many studies of electronic, optical and thermoelectric properties has been reported for the alkaline element based HH alloys. P.K. Kamlesh et al., (2021) studied various properties including thermoelectric and optical properties of the XScZ (X = Li, Na, K; Z = C, Si, Ge) half-Heusler compounds. They conclude that these alloys can be used for photovoltaic devices and they are suitable candidates for thermoelectric applications because these materials are semiconductor with direct gap and there are optically active in the near infrared and visible range and they also exhibit high merit factor. Y. Cherchab and R.G. Hernandez (2021) have studied the structural stability of KLaX (X = C, Si, Ge, and Sn) half-Heusler alloys within the TB-MBJ method both with and without spin–orbit interaction. A semiconductor nature with direct band gaps was observed and the spin–orbit coupling has increased the flatness of the valence band for X = Si to Sn. The high values of merit factor and thermopower make these alloys promising materials for thermoelectric applications. Based on DFT calculations, R.Ahmed et al., (Ahmed et al. 2017) have found ZT values close to unity for the LiMgN, NaMgN and KMgN half-Heusler compounds, thus revealing that these materials could be useful for thermoelectric applications and also used as an alternative green energy resources. By the tight binding linear muffin-tin orbital (TB-LMTO) method within the local spin density approximation (LSDA), R. Umamaheswari et al., (Umamaheswari et al. 2014) have demonstrated the robustness of half metallicity against the lattice contraction for the XCaB and XSrB (X = Li, Na and K) alloys. The main motivation of this study is inspired by the promising applications of HH alloys in the area of optoelectronics and energy conversion. The relevance of the half-Heusler RbScSn for its use in optical and thermoelectric devices will be investigated because until today, there is no experimental or theoretical data about this compound.

2 Computational method

The structural, electronic, optical and thermoelectric properties of RbScSn half-Heusler (H.H) have been investigated with WIEN2k code (Blaha and al., WIEN2K, 2001), which is based on the density functional theory (DFT) method (Hohenberg and Kohn 1964). The calculations has been done using the full potential linearized augmented plane wave (FP-LAPW) method (Singh 1994). The exchange–correlation effects were treated with generalized gradient approximation (GGA) (Perdew et al. 1996; Wu and Cohen 2006) and the Tran-Blaha modified Becke-Johnson (TB-mBJ) exchange potential (Tran and Blaha 2009). The H.H have the C_{1b} crystal structure with the space group F-43 m (Fig. 1). The Brillouin zone integration is performed with $15\times15\times15$ Monkhorst–Pack mesh points (Monkhorst and Pack 1976). The muffin tin radius (R_{MT}) values was set as 2.5 a.u, 2.1 a.u and 1.9 a.u for Rb, Sc and Sn atoms, respectively. Other parameters such as spin cut off $R_{MT.}K_{max}$, cut-off energy, Gaussian parameter (Gmax) and the maximum value of angular momentum (lmax) are taken to be respectively 7.0, -6 Ry, 12 $(a.u)^{-1}$ and 10. The convergence criterion of the self-consistent calculation cycles was selected as 10^{-4} Ry. The phonon frequencies were calculated using the density functional perturbation theory (DFPT) with $2\times2\times2$ supercells (Shang et al. 2017). The optical constants are derived from the complex dielectric function (Adachi 2009; Sun et al. 2004; Hu et al. 2007). To investigate the thermoelectric response of RbScSn compound, the semi-classical Boltzmann approach as given in the BoltzTraP code (Madsen et al. 2006) was used under a fine grid mesh ($46\times46\times46$) in order to accurate values of the electronic velocities, which is a crucial parameter involved in the Boltzmann theory (Allen 1996). The explicit valence electrons for the RbScSn primal cell are $5s^1$ of Rb, $3d^1\ 4s^2$ of Sc and $4d^{10}\ 5s^2\ 5p^2$ of Sn.

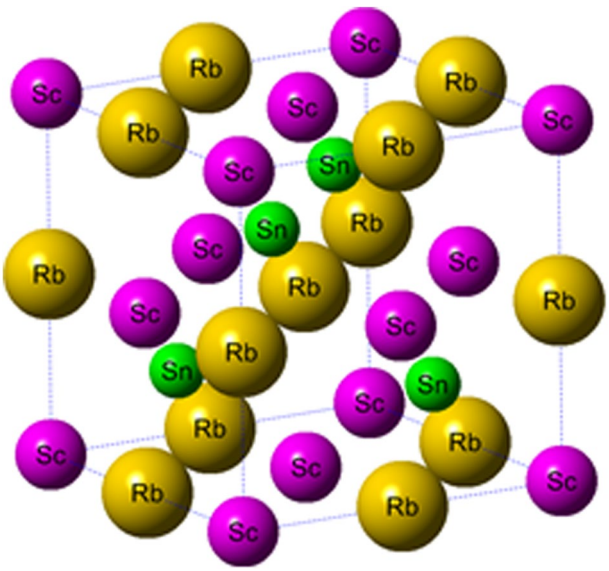

Fig. 1 Cubic structure of RbScSn compound

Table 1 The positions of Rb, Sc and Sn atoms in three possible atomic arrangements

Phase	Rb	Sc	Sn
α	(1/2, 1/2, 1/2)	(0, 0, 0)	(1/4, 1/4, 1/4)
β	(1/4, 1/4, 1/4)	(1/2, 1/2, 1/2)	(0, 0, 0)
γ	(0, 0, 0)	(1/4, 1/4, 1/4)	(1/2, 1/2, 1/2)

Table 2 Calculated structural equilibrium lattice constant a_0, bulk modulus B, its pressure derivatives B', ground state energies E_{min}, formation energy ΔH_f and cohesive energy E_{coh} of the cubic RbScSn

Space group	State	Phase	a_0 (Å)	B (GPa)	B'	E_{min} (Ry)	ΔH_f (eV/atom)	E_{coh}(eV/atom)
F-43 m	NM	α	7.72	23.85	5.81	− 19,849.607982	− 0.348	− 6.6967
	NM	β	7.56	18.45	4.27	− 19,849.468665	1.547	− 4.7892
	NM	γ	7.44	25.16	3.81	− 19,849.607356	− 0.339	− 6.6803
	FM	α	7.71	26.32	3.93	− 19,849.607901	− 0.346	− 6.6953
	FM	β	7.56	18.48	4.41	− 19,849.468668	1.547	− 4.7892
	FM	γ	7.43	25.15	3.80	− 19,849.598861	− 0.223	− 6.5715
	AFM	α	7.71	26.32	3.93	− 19,849.606227	− 0.324	− 6.6667
	AFM	β	7.55	17.55	3.83	− 19,849.468608	1.548	− 4.7892
	AFM	γ	7.43	27.61	3.91	− 19,849.606418	-0.326	− 6.6667

3 Results and discussions

3.1 Structural properties and phase stability

The RbScSn HH crystallize in the face-centered cubic (FCC) structure, type MgAgAs with F-43 m (216) space-group where, Rubidium, Scandium and Tin occupies (1/2, 1/2, 1/2), (0, 0, 0) and (1/4, 1/4, 1/4) site respectively (Table 1). The structural equilibrium lattice constant, bulk modulus, its pressure derivatives and ground state energies in the ferromagnetic (FM), nonmagnetic (NM) and antiferromagnetic (AFM) configurations are reported in Table 2. The optimization results found among the nine possible atomic arrangement shows that the NM state in the phase "α" provides lowest energy. The lattice parameter found which is 7.721 Å is in adequacy with those of other semi-heusler compounds where the element which occupies the X position is an alkali, like RbYSn (7.768 Å) (Hoat and Naseri 2020), RbCaAl (7.776 Å) (Umamaheswari et al. 2014) and KScGe (7.128 Å) (Ciftci and Mahanti 2016). From Fig. 1, which display the unit cell structure of RbScSn compound plotted by using the CrystalMaker 2.7 software (Crystalmaker software, crystalmaker, online xxxx), one can see that the configuration consist of three interpenetrating ordered fcc sublattices. The Sc and Rb occupy the octahedral and tetrahedral sites as a cation, while Sn occupies the octahedral sites as an anion. In order to predict if the RbScSn HH may be synthesized experimentally, we have computed the formation energy ΔH_f according to the relation (1) (Amudhavalli et al. 2018):

$$\Delta H_f = E_{\mathrm{XYZ}}^{\mathrm{tot}} - \left(E_X^{\mathrm{bulk}} + E_Y^{\mathrm{bulk}} + E_Z^{\mathrm{bulk}}\right) \quad (1)$$

where E_{XYZ}^{tot} is the total energy of primitive cell and E^{bulk} is the energy per atom of constituent atoms in bulk. The negative value of − 0.348 (eV/atom) confirms that the synthesis of

RbScSn alloy is possible. In the same context, to predict the structural stability of RbScSn compound, the cohesive energy were calculated according to the relation (2) (Gueorguiev et al. 2005):

$$E_{coh} = E_{XYZ}^{tot} - \left(E_X^{iso} + E_Y^{iso} + E_Z^{iso}\right) \quad (2)$$

where E^{iso} is the energy of isolated atom.

The negative value of − 0.4916 (eV/atom) confirms that the RbScSn alloy is structurally stable.

The phonon distribution spectrum (PDS) of RbScSn compound is computed using the density functional perturbation theory (DFPT) based linear response method. A supercell of 2 × 2 × 2 primary cells was built (Shang et al. 2017). By using the Phono3py code (Togo and Tanaka 2015) the calculated PDS along the high-symmetry points in the first Brillouin zone Γ-X-K-Γ-L-X-W-L is shown in Fig. 2. This curve show nine vibrational modes, three acoustic modes and six optical modes since there are three atoms in the primitive unit cell. The frequency of the acoustic modes of vibration occurs between [0—2.78 THz] while the frequency of the optical modes exists above the frequency of 2.24 THz. The maximum frequency of acoustic modes is 2.45 THz (in Γ – X direction) and the minimum frequency of optical modes is 2.18 THz (in K – Γ direction). The obtained phonon curve of our compound, is consistent with the phonon curves of NiHfSn, PdHfSn, PtHfSn compounds (Nagura et al. 2021). A splitting is observed at the Γ-Γ point, this characteristic is common in ionic semiconductors (Eliassen et al. 2017). The RbScSn compound is dynamically stable due to the positive vibration mode values (no imaginary modes).

3.2 Electronic properties

In order to better understand the electronic structure of the already optimized RbScSn compound, the calculation of its energy band structure and its density of electronic state is considered necessary. The illustration in Fig. 3 gives the electronic band structure of RbScSn in the energy region between -3 and 6 eV. We can see that the Fermi energy is on the top of the valence band and the band gaps calculated by GGA and mBJ are 0.434 eV

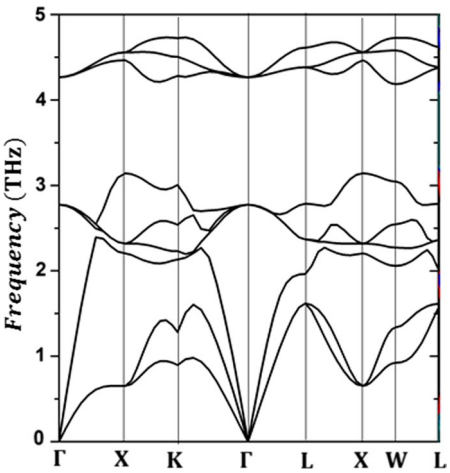

Fig. 2 The phonon dispersion curve for RbScSn

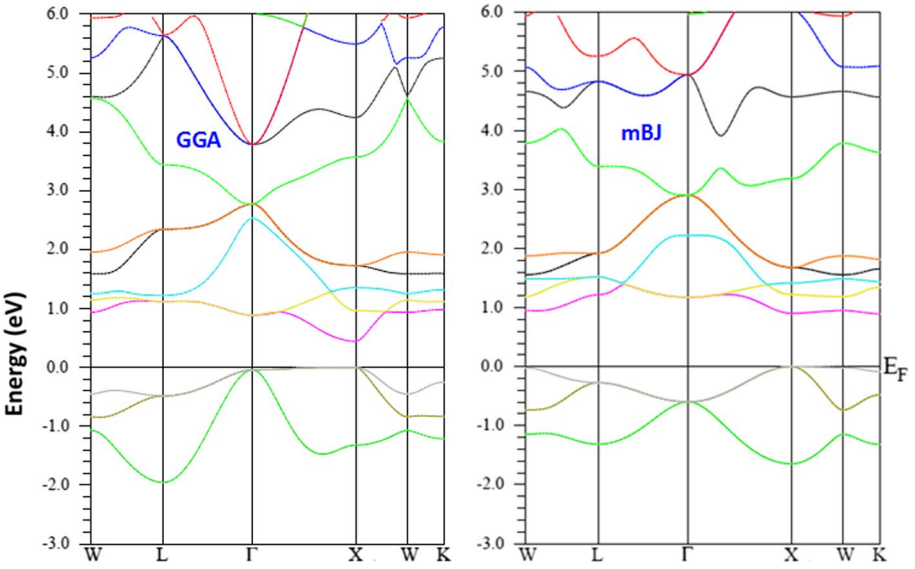

Fig. 3 Band structure of RbScSn compound **a** GGA and **b** TB-mBJ

and 0.895 eV, respectively. An improvement around 100% of the band gap by TB-mBJ approach is clearly noted. This result has also been noticed in many half-Heusler alloys such as TiIrBi (Candan and Kushwaha 2021), BaAgP (Parvin et al. 2021), HfRhSb (Rajendran 2022). We have found that the RbScSn is a semiconductor with direct band gap since the conduction band minimum (CBM) and valence band maximum (VBM) are located at the same symmetry point X. The total magnetic moment obtained by both approximations (GGA and TB-mBJ) is found equal to zero, from where the RbScSn is nonmagnetic material. This confirms the already result obtained by the band structure diagrams, which exhibit the same profile for spin up and spin down channel. The energy levels in the valence band exhibit a high curve slope, which translates to high group velocity and low effective mass of electrons (TB-mBJ case). Around the Fermi level, the electrons are extremely lightweight, so that in the Γ-X region the effective electron mass is small and the corresponding group velocity is important. Whereas in the GGA case and always around the Fermi level, there is a very small slope of the plot in the Γ-X region, which mean a large effective electron mass and a corresponding group velocity almost zero (Nourozi et al. 2019). Both GGA and mBJ calculations have given for the conduction band the same report; an important slope gradient along the X symmetry point in the Γ-X region, which mean a low effective mass and high group velocity for electron. The atomic disposition in the unit cell as well as the electrons engaged in the shaping of the forbidden band require the plot of the total and partial density of electronic states (TDOS/PDOSs). The plots in Fig. 4 depicts between − 3 and 6 eV, the TDOS/PDOSs of RbScSn alloy, where the dashed line shows the Fermi energy level (EF). The valence band located between -1 and 1 eV comes from the hybridization of Sc-d states and Sn-p states. Between −2 and −1 eV, the valence band comes mainly from a major contribution of Sn-p states and a minor contribution of Sc-d states. The energy domain located among 0 and 6 eV constitutes the conduction band, it is distinguished by the appearance of gap (0.895 eV) produced from the contribution of the Sc-d state and Sn-p state. The contribution from the Rb atom nearby the

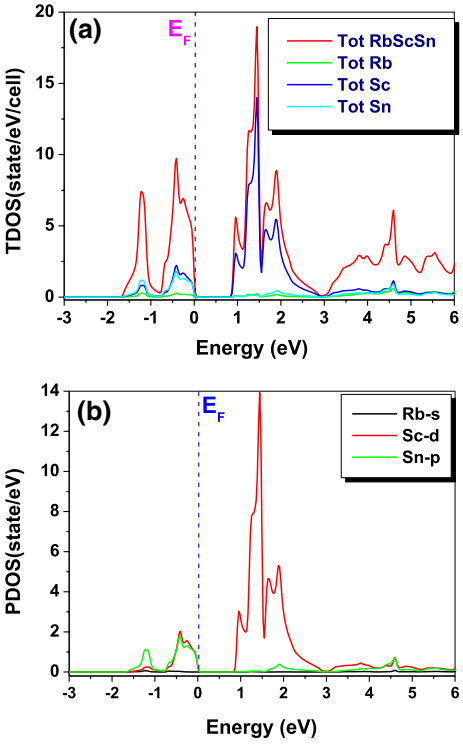

Fig. 4 Total and partial density of states (TDOS/PDOS) of RbScSn

VBM and CBM is very weak. This indicates that the thermoelectric properties are mainly encouraged only by the Sc and Sn atoms. We can conclude that the electronic properties of the RbScSn alloy are in very agreement with some results available on half-Heusler semiconductors with an alkaline element, like KScGe, NaScSi (Kamlesh et al. 2021) and RbYSn (Hoat and Naseri 2020).

3.3 Elastic properties

To investigate the mechanical stability of cubic half-Heusler RbScSn, it is necessary to calculating the independent elastic constants C_{11}, C_{12}, C_{44} (Hornstra and Bartels 1978). These constants are employed to evaluate some mechanical parameters such as, the bulk modulus *B,* the shear modulus *G,* Young's modulus *E,* Poisson's ratio ν and the elastic anisotropy factor *A* as follows (Wang and Ye 2003):

$$B = \frac{1}{3}\left(C_{11} + 2C_{12}\right) \quad (3)$$

$$G = \frac{C_{11} - C_{12} + 3C_{44}}{5} \quad (4)$$

$$E = \frac{9BG}{3B+G} \quad (5)$$

$$\nu = \frac{3B-E}{6B} \quad (6)$$

$$A = \frac{2C_{44}}{C_{11}-C_{12}} \quad (7)$$

From the obtained values of the elastic constants (Table 3) we can say that the mechanical stability which is governed by Born-Huang criteria (Born and Huang 1954) (C_{11}–$C_{12}>0$); ($C_{11}+2C_{12}>0$); ($C_{11}>0$); ($C_{44}>0$) and ($C_{12}<B<C_{11}$) is completely satisfied. In other words, this means that at zero pressure, the cubic structure of the RbScSn is mechanically stable. The obtained value of C_{11}, which is greater than those of C_{12} and C_{44}, indicate that the RbScSn is more resistant to the unidirectional compression than shear deformation (Cheriet et al. 2021). The low value obtained for the bulk modulus (*B*) shows that the RbScSn compound is easy to compress. Shear modulus (G) is an index of variation in angle of bond when the stress is applied; its value for the RbScSn is of 6.34 GPa, while the Young's modulus (E) is about 16.64 GPa. Based on the calculated values of G and E, we can conclude that the RbScSn is soft material with low rigidity. The order of magnitude of G and E found for our compound are established also in several compounds cited in the literature (Hornstra and Bartels 1978; Shakil et al. 2022). The Poisson's ratio (ν) value obtained for RbScSn which is of 0.31 confirms the presence of covalent and metallic bonding, because according to Haines et al. (Haines et al. 2001) this bonding nature occurs as long as $\nu < 0.33$. In addition, our compound have an anisotropy factor (A) which deviates largely from the unity, which indicates that it is an elastic anisotropic material, but this degree of anisotropy is low therefore the risk of micro cracking is very minimal. The ductility and fragility of a material are estimated using the Pugh B/G criterion (Pugh and XCII. 1954). The materials are ductile for B/G > 1.75 and brittle for B/G < 1.75. The obtained value of B/G for the RbScSn is of 2.31, value greater than 1.75, which means that our material is ductile (Table 3).

3.4 Optical properties

In order to describe the interaction of photons with RbScSn half-Heusler, the calculation of optical properties is necessary. The most of the optical properties derive from the complex dielectric function $\varepsilon(\omega)$ (Eq. 8) (Adachi 2009).

$$\varepsilon(\omega) = \varepsilon_1(\omega) + i\varepsilon_2(\omega) \tag{8}$$

where $\varepsilon_1(\omega)$ represents the real transition between the occupied and unoccupied states while $\varepsilon_2(\omega)$ depicts the electronic polarizability under incident light (Amin et al. 2011). The imaginary part of the dielectric function $\varepsilon_2(\omega)$ is derived from the electronic band structure computations with the help of the following relation

$$\varepsilon_2(\omega) = \left(\frac{4\pi^2 e^2}{m^2\omega^2}\right) \sum_{i,j} \int \langle i|M|j\rangle^2 f_i\left(1-f_i\right)\delta\left(E_j - E_i - \omega\right) d^3k \tag{9}$$

where $e, m, \omega$and$M$ represent the electron charge, electron mass, photon frequency and dipole matrix, respectively. E_i is the electron energy of the initial state, E_j is the electron energy of the final state and f_i is the Fermi occupation factor of the single-particle state i. The real part $\varepsilon_1(\omega)$ of the dielectric function derives from $\varepsilon_2(\omega)$ by using the Kramers Kronig relations (Marius 2010; Gajdoš et al. 2006; Ambrosch-Draxl and Sofo 2006):

$$\varepsilon_1(\omega) = 1 + \frac{2}{\pi} P \int_0^{\infty} \frac{\omega' \varepsilon_2(\omega')}{\omega'^2 - \omega^2} d\omega' \tag{10}$$

where P is the Cauchy principal value.

Table 3 The computed elastic constants (*Cij*), bulk modulus (*B*), Shear modulus (*G*), Young's modulus (*E*), Poisson's ratio (ν), anisotropic factor A, and Pugh's ratio (*B/ G*) of RbScSn half-Heusler

$C_{11}(GPa)$	$C_{12}(GPa)$	$C_{44}(GPa)$	$B(GPa)$	$G(GPa)$	$E(GPa)$	ν	A	B/G
24.994	9.571	5.436	14.712	6.346	16.644	0.311	0.704	2.318

Other optical parameters like the absorption coefficient $a(\omega)$, reflectivity $R(\omega)$ and refractive index $n(\omega)$ can be obtained from the calculated values of the real and imaginary parts of the dielectric function (Irfan et al. 2019):

$$a(\omega) = \frac{\sqrt{2\omega}}{c}\left(\sqrt{\varepsilon_1^2(\omega)+\varepsilon_2^2(\omega)}-\varepsilon_1(\omega)\right)^{1/2} \quad (11)$$

$$R(\omega) = \left|\frac{\sqrt{\varepsilon(\omega)}-1}{\sqrt{\varepsilon(\omega)}+1}\right|^2 \quad (12)$$

$$n(\omega) = \left[\frac{\sqrt{\varepsilon_1^2(\omega)+\varepsilon_2^2(\omega)}+\varepsilon_1(\omega)}{2}\right]^{1/2} \quad (13)$$

As the lattice parameters are constant (cubic structure), the obtained optical properties are isotropic (same dielectric tensor). A dense k-point mesh of (31*31* 31) was used in order to achieve reasonable precision of all possible transitions. The diverse optical properties calculated by TB-mBJ approach was plotted in the ultraviolet (UV), visible (Vis), and near infrared NIR) ranges (0–14 eV). Figure 5a depicts the evolution of the real part $\varepsilon_1(\omega)$ and imaginary part $\varepsilon_2(\omega)$ of the dielectric function $\varepsilon(\omega)$ in the energy range from 0 to 14 eV. The limit value $\varepsilon_1(0) = 75.65$, which corresponds to the irradiation frequency close to zero is designated the static dielectric constant. The obtained result of the real part $\varepsilon_1(\omega)$ show that the zero crossing of the spectrum means the non-existence of scattering. Between [0.91–1.04 eV], [2.29–2.43 eV] and [4.63–8.83 eV], $\varepsilon_1(\omega)$ exhibits negative values which means that the electromagnetic waves in these energy ranges will be reflected by the medium; hence, the material exhibits metallic character. The fluctuations observed in the real part of the dielectric function correspond to the local maxima of absorption or reflectivity. Analysis of the $\varepsilon_2(\omega)$ spectrum shows that the first critical point, which corresponds to the fundamental absorption threshold, starts at around 0.12 eV. The origin of this point correlate with an optical transition, which occurs between the maximum of the valence band, located at (X) and the minimum of the conduction band located at (X). The main peak, which occurs at 0.23 eV is due to the transition of electrons from Sn-p and Sc-d states of the valence band to the unoccupied states in the conduction band. The profile of the real and imaginary part of the dielectric function of RbScSn compound attenuates in the UV domain; this result is also observed in many semiconductor such as $Al_xGa_{1-x}P$ (Zafar et al. 2019) and ($In_xGa_{1-x}N$Shakil et al. 2018). Figure 5b gives the variation of the absorption coefficient $a(\omega)$ versus photon energy. The light absorption in the visible range extends from 28.51×10^4 cm^{-1} at 1.7 eV (red color) to 41.69×10^4 cm^{-1} at 3.17 eV (violet color) and the maximum value of 54.86×10^4 cm^{-1} occurs at 2.29 eV (green color). The rapid growth of $a(\omega)$ between 0.0 eV and 4.7 eV is an observation often met in materials with semiconductor behavior. The maximum absorption coefficient of 113.82×10^4 cm^{-1}, registered at 4.67 eV (ultraviolet region) leads to conclude that the RbScSn half-Heusler can be used as absorber of harmful UV radiations. In addition, due to the absorption, which

occurs over a wide range of energy, this compound is likely to be used as a low intensity electromagnetic wave shielding (Forozani et al. 2020). The phenomenon of change of direction of a light ray during its passage from one given optical medium to another, due to a change in the speed of its propagation is known as refraction. From Fig. 5c which gives us the refractive indices $n(\omega)$, one can observe that the profile of $n(\omega)$ is analogous to that of $\varepsilon_1(\omega)$. At zero frequency, the real part of the dielectric constant $\varepsilon_1(0)$ and the refractive index $n(0)$ are conform to ($\varepsilon_1(0) = n^2(0)$Poelman and Smet 2003). The $n(\omega)$ decreases at very low energies then fluctuates in the visible—ultraviolet range until it stabilizes around 1 for energies equal or greater than 5.22 eV. The maximum value of $n(\omega)$ in the visible domain is found as 3.44. The reflectivity $R(\omega)$ expressed as a percentage, defines the ratio between the reflected luminous flux and the incident luminous flux. The different peaks reveal that the photons are reflected on the surface of the material. At zero energy, $R(0)$ is quite high, its value is of 63% Fig. 5d. Above low energies, $R(\omega)$ fluctuates and reaches its maximum of 48% in the UV domain, its most value in the visible range (1.7–3.3 eV) is around 43%. The RbScSn is a good reflector of infrared radiation, its value is of (64%), it is clearly better than that obtained by other Half-heusler compounds, recently studied such as RhTiSb (29%) (Besbes et al. 2019), FeCrAs (31%) (Djelti et al. 2020), SiLiCa (36%) (Djelti et al. 2021), AgScSi (41%) (Durukan and Ciftci 2019) and NaScSi (42%) (Durukan and Ciftci 2021). This high reflectivity in the near infrared range makes half-Heusler RbScSn an ideal material for high performance heat shields. From Fig. 5e, which depicts the energy loss function L(ω), we can see that there is no significant peak in visible and near infrared. This can be explained by the fact that $\varepsilon_2(\omega)$ still has large values in these domains (Benahmed et al. 2017). In the energy range considered in this research, $L(\omega)$ reaches its maximum peak of about 1.67 at 11.07 eV (UV-domain), this peak correspond to the rapid decrease in the reflectivity spectrum $R(\omega)$. The range of frequencies corresponding to this peak is called the Plasmon frequency. In the visible range the maximum $L(\omega)$ is about 0.20. The static values calculated for the dielectric constant $\varepsilon_1(0)$, refractive index $n(0)$ and reflectivity $R(0)$ of RbScSn compound are given in Table 4. Unfortunately, there are no experimental data available of band gap and static dielectric constant of the RbScSn compound, then the first principles prediction remain the only suitable tool for obtaining such important information.

3.5 Thermoelectric properties

In this section, the transport properties are going to be computed with BoltzTraP code (under a constant relaxation time approximation of the charge carriers) (Allen 1996). The thermoelectric characteristics such as the electrical conductivity (σ/τ), thermal conductivity (κ/τ), Seebeck coefficient (S) and Merit factor (ZT) are investigated versus the change in chemical potential, change which can influences the stability of the materials during doping even if the electronic band remains unchanged (Bik et al. 2006; Gupta et al. 2022; Kumar and Roy 2018). Semi-classical Boltzmann transport equations are used to calculate the number of thermoelectric coefficients, which can be represented as follows (Vasileska et al. 2011; Reshak 2016):

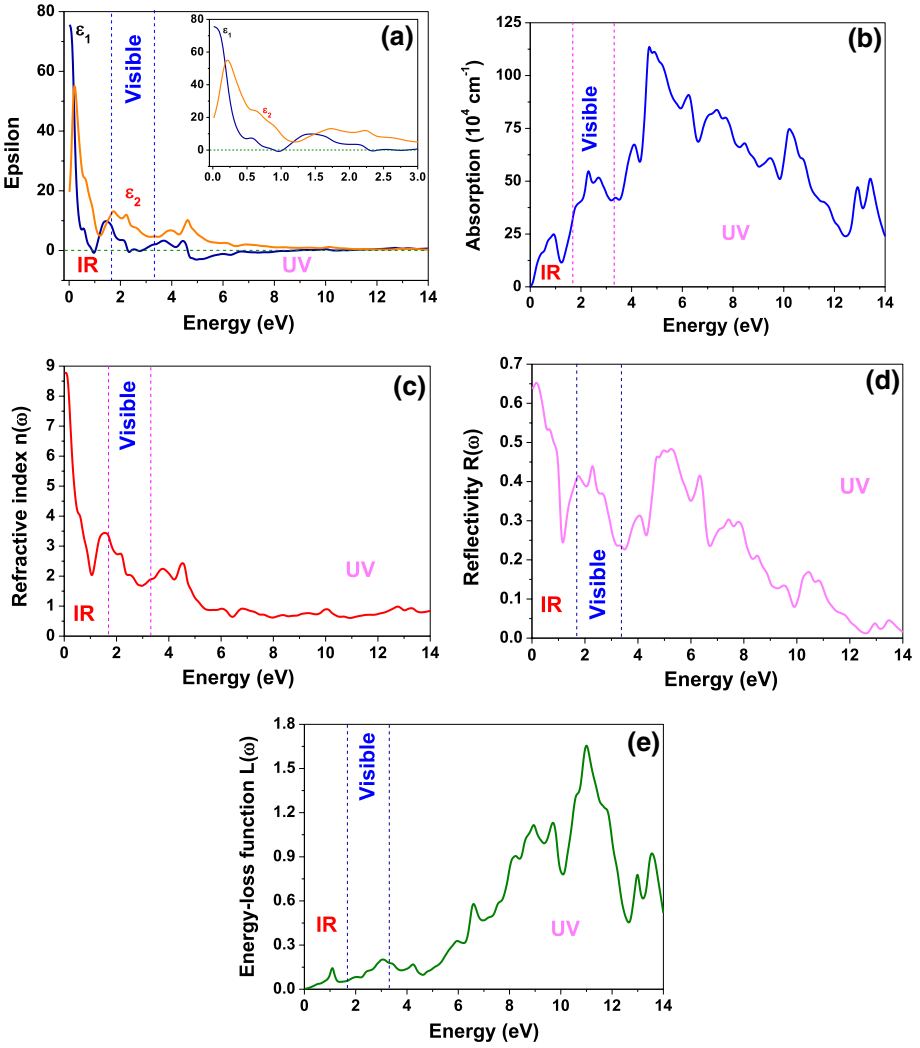

Fig. 5 Illustration of **a** real $\varepsilon_1(\omega)$ and **b** imaginary $\varepsilon_2(\omega)$ component of dielectric function, **c** absorption coefficient a(ω), **d** refractive index n(ω), **e** reflectivity R(ω) and **f** electron energy loss L(ω) of cubic RbScSn compound

$$\sigma_{\alpha\beta}(T,\mu) = \frac{1}{\Omega}\int \sigma_{\alpha\beta}(\varepsilon)\left[-\partial f_{\mu}(T,\varepsilon)\right]d\varepsilon \quad (14)$$

$$\kappa_{\alpha\beta}(T,\mu) = \frac{1}{e^2T\Omega}\int \sigma_{\alpha\beta}\varepsilon(\varepsilon-\mu)^2\frac{\partial f_{\mu}(T,\varepsilon)}{d\varepsilon} \quad (15)$$

$$S = \frac{e}{T\sigma}\int \sigma_{\alpha\beta}(\varepsilon)(\varepsilon-\mu)\left[\frac{-\partial f_{\mu}(T,\varepsilon)}{\partial\varepsilon}\right] \quad (16)$$

$$\mathrm{ZT} = \frac{S^2\sigma T}{\kappa} \quad (17)$$

where Ω, f, μ, σ, κ, S and Z represents the unit-cell volume, Fermi–Dirac distribution function, chemical potential, electrical conductivity, thermal conductivity, Seebeck coefficient and merit factor respectively. The Seebeck coefficient (S) is important criteria of

the electronic structure of a material near the Fermi level. From Fig. 6a, which depicts S versus chemical potential (μ), we can see that the utmost value decreases with increasing the temperature, it goes from 231.25 μV/K at 300 K to 196.88 μV/K at 900 K. The optimal value of S (both positive and negative) at 300, 600 and 900 K occurs at positive side of μ. The Seebeck values obtained versus temperature exhibit a maximum value of 240.18 μV/K at 200 K then it declines abruptly up to 1200 K. All the values are positive which suggests that the conductivity is done through the holes, hence the half-Heusler RbScSn is an n-type semiconductor. The variation of the electrical conductivity (σ/τ) versus chemical potential (μ) for different temperatures is depicted in Fig. 6b. In the range of chemical potential considered in this research (−0.16 to 0.18 eV), we can notice that (σ/τ) is higher in p-type side than in n-type side. The electrons in *p*-type region have shown dominancy with maximum peak intensity value of 1.58×10^{20} $(\Omega\ \mathrm{m\ s})^{-1}$ observed at 0.12 eV, while in the n-type side, the peak intensity is about 1.41×10^{20} $(\Omega\ \mathrm{m.s})^{-1}$. The minimum values of (σ/τ) for the different temperatures are located between μ = 0 and 0.03 eV. In addition, we can observed that there is no important change in the electrical conductivity, when the temperature moved from 300 to 900 K; the three curves are almost confused. The high electrical conductivity values obtained for the RbScSn imply that the losses through the Joule effect will be weak. This statement can be explain by the fact that the effective masses of holes (valence band) are lighter than the effective masses of electrons (conduction band). Figure 6c, which gives the thermal conductivity (κ) plotted against chemical potential μ (eV) reveals a noticeable amplification of κ occurs with the increase in temperature values.

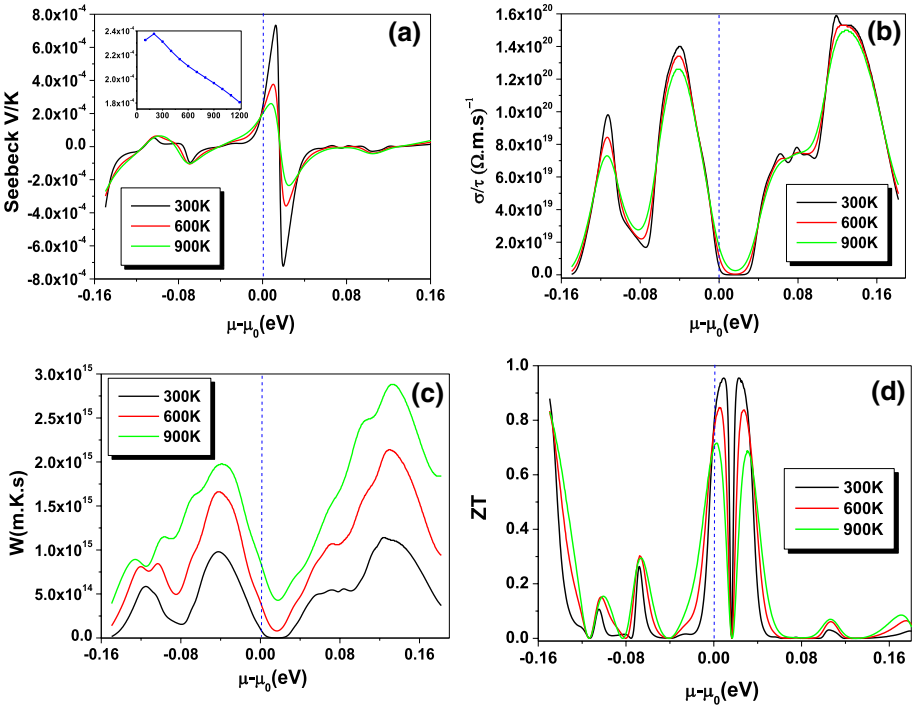

Fig. 6 Evolution versus chemical potential at different temperature of **a** Seebeck coefficient, **b** Electrical conductivity, **c** thermal conductivity and **d** the merit factor of cubic RbScSn compound

Table 4 Calculated band gap, static dielectric constant $\varepsilon_1(0)$, static refractive index $n(0)$ and static reflectivity $R(0)$ for RbScSn performed with TB-mBJ calculation

Alloy	Approximation	Gap (eV)	$\varepsilon_1(0)$	$n(0)$	$R(0)$
RbScSn	TB-mBJ	0.434 (GGA) 0.895 (mBJ)	75.89	8.75	0.63

The highest values are obtained at 900 K while the lower values occurs at 300 K. In addition, the κ is dominant for the electrons (n-type) than holes (p-type). The thermal conductivity value at ambient temperature is $1{,}13.10^{15}$ W/m.K.s in n-type and $9{,}83.10^{14}$ W/m.K.s in p-type. In addition, κ remains low in a wide range of chemical potentials, which corresponds to good thermoelectric efficiency (high ZT) in this region. For the other values of μ, we observe an increase of κ with temperature and with chemical potential. The κ value is large for positive chemical potential than negative chemical potential. The behavior of thermal conductivity at room temperature is found to be similar as those already reported in several studies of half-Heusler semiconductors such as KLaX (X = Si and Ge) (Cherchab and Hernandez 2021), RbYSn (Hoat and Naseri 2020). In order to estimate the thermoelectric efficiency of RbScSn half-Heusler, we calculated the fluctuation of the merit factor (ZT). Figure 6d, gives ZT plotted against chemical potential μ (eV) at different temperature. The ZT values are more prominent in n-type region than the p-type region and as the temperature increases, the maximum value of ZT gradually decreases. The maximum value of ZT is 0.97, 0.85 and 0.72 at 300 K, 600 K, and 900 K respectively. For chemical potential values greater than (0 eV) and lower than (0.03 eV), the ZT value decrease, due to a high Seebeck coefficient, a high thermal conductivity and low electrical conductivity. At ambient temperature, our half-Heusler shows a ZT value around the unity (0.97), which allows us to conclude that RbScSn is one of the most suitable materials for thermoelectric applications at room temperature because the ZT value close to unity is preferable to obtain a high efficiency of thermoelectric devices. We identified in the literature several good thermoelectric material, which exhibit a ZT values slightly small than those of RbScSn alloy, such as KLaC (Cherchab and Hernandez 2021), ScAuSi (Abraham et al. 2021), PtXSn (X = Zr, Hf) (Khandy et al. 2021), LuNiSb (Saini 2021), ZrRhSb (Khandy 2021), TaIrGe (Hussain et al. 2020).

4 Conclusion

The first-principle calculations were used to investigate the electronic, optical and thermoelectric properties of the new stable half-Heusler RbScSn. The full potential linearized augmented plane wave (FP-LAPW) method with the generalized gradient approximation (GGA) and modified Becke–Johnson (mBJ) approximation have been used. The predicted phonon dispersion does not present any imaginary frequencies and the calculation of mechanical properties revealed that the material is mechanically stable. The formation and cohesive energies are negatives, which confirms that the RbScSn half-Heusler is energetically and dynamically stable and that its synthesis is possible. The band structures obtained by the two approximations shows a semiconductor behavior characterized by a direct band gap of about 0.895 eV (mBJ)/0.434 eV (GGA). The RbScSn alloy exhibit

maximum absorptivity and minimum reflectivity in the ultraviolet range, which suggests a possibility of using it as an absorber of harmful UV radiation. Also the high reflectivity obtained in the near infrared range makes RbScSn as an ideal material for high performance heat shields. The variation of thermoelectric properties as a function of chemical potential at different temperatures (300, 600 and 900 K) were assessed using calculations of the Seebeck coefficient, electrical conductivity, thermal conductivity and merit factor. The temperature effect is relatively large on thermal conductivity than on the other three properties. In all the temperature range considered in this research, the overall behavior of Seebeck coefficient shows a positive variation which means that the n-type charge carriers are dominant. The high values of Seebeck coefficient (734 $\mu V/K$) and electrical conductivity $\left(1.41 \times 10^{20} (\Omega \text{ m s})^{-1}\right)$ and the low value of thermal conductivity $\left(9.1 \times 10^{14} \text{m K s}\right)$ obtained at 300 K give a ZT value close to unity, which reveals that the RbScSn is a suitable material for thermoelectric applications at room temperature. Most of electronic, optical and thermoelectric parameters obtained for RbScSn were confronted with those given by semiconducting half-Heusler compounds, a good agreement were found.

Funding We declare that we do not have any financial and personal conflict of interest with other persons or organizations that could inappropriately influence our work.

Declarations

Conflict of interest All the authors of this manuscript are agree with the submission of manuscript.

References

Abraham, J.A., Sharma, R., Ahmad, S., Dey, A.: DFT investigation on the electronic, optical and thermoelectric properties of novel half-Heusler compounds ScAuX (X = Si, Ge, Sn, Pb) for energy harvesting technologies. Eur. Phys. J. plus **136**, 1091 (2021)

Acharya, M., Jana, S.S., Ranjan, M., Maiti, T.: High performance (ZT>1) n-type oxide thermoelectric composites from earth abundant materials. Nano Energy **84**, 105905 (2021)

Adachi, S.: Properties of Semiconductor Alloys: Group-IV III-V and II-VI Semiconductors. Wiley, London (2009)

Ahmed, R., Masuri, N.S., Haq, B.U., Shaari, A., AlFaifi, S., Butt, F.K., Muhamad, M.N., Ahmed, M., Tahir, S.A.: Investigations of electronic and thermoelectric properties of half-Heusler alloys XMgN (X = Li, Na, K) by first-principles calculations. Mater. Des. **136**, 196–203 (2017)

Allen, P.: Boltzmann Theory and Resistivity of Metals. Kluwer International Series in Engineering and Computer Science, pp. 219–250. Springer, Boston (1996)

Ambrosch-Draxl, C., Sofo, J.O.: Linear optical properties of solids within the full potential linearized augmented planewave method. Comput. Phys. Commun **175**, 1–14 (2006)

Amin, B., Ahmad, I., Maqbool, M., Goumri-Said, S., Ahmad, R.: Ab initio study of the bandgap engineering of $Al_{1-x}Ga_xN$ for optoelectronic applications. J. Appl. Phys. **109**, 023109 (2011)

Amiri, P., Shavi, Z.D., Aliakbari, A., Salehi, H.: The investigation of the half-metallic properties of half Heusler KXP (X = Cr & Mo) compounds: a first-principles study. J. Phys. Chem. Solids **160**, 110294 (2022)

Amudhavalli, A., Rajeswarapalanichamy, R., Iyakutti, K.: Half-metallic ferromagnetism in Ni based half Heusler alloys. Comput. Mater. Sci. **148**, 87–103 (2018)

Benahmed, A., Bouhemadou, A., Khenata, R., Bin-Omran, S.: Ab initio study of the electronic, optical and thermodynamic properties of the ternary phosphides LiAeP (Ae = Sr, Ba). Indian J. Phys. **91**, 157 (2017)

Besbes, A., Djelti, R., Bestani, B.: Optical and thermoelectric response of RhTiSb half-Heusler. Int. J. Mod. Phys. B **33**(22), 1950247 (2019)

Bik, D.I., Mahanti, S.D., Kanatzidis, M.G.: Ab initio studies of the electronic structure of defects in PbTe. Phys. Rev. B **74**, 155205 (2006)
Blaha, P. and al., WIEN2K, An Augmented Plane Wave+ Local Orbitals Program for Calculating Crystal Properties, edited by K. Schwarz, Vienna University of Technology, Austria, 2001.
Born, M., Huang, K.: Dynamics Theory of Crystal Lattices. Oxford University Press, Oxford (1954)
Bos, J.W.G., Downie, R.A.: half-Heusler thermoelectric: a complex class of materials. J. Phys. Condens. Matter **26**, 433201 (2014)
Candan, A., Kushwaha, A.K.: A first-principles study of the structural, electronic, optical, and vibrational properties for paramagnetic half-Heusler compound TiIrBi by GGA and GGA + mBJ functional. Mater. Today Commun. **27**, 02246 (2021)
Chen, S., Ren, Z.: Recent progress of half-Heusler for moderate temperature thermoelectric applications. Mater. Today **16**, 387–395 (2013)
Cherchab, Y., Hernandez, R.G.: Structural stability and thermoelectric properties of new discovered half-Heusler KLaX (X = C, Si, Ge, and Sn) compounds. Comput. Theor. Chem. **1200**, 113231 (2021)
Cheriet, A., Khenchoul, S., Aissani, L., Lagoun, B., Zaabat, M., Alhussein, A.: First-principles calculations to investigate structural, magnetic, electronic and elastic properties of full-Heusler alloys Co_2MB (M=V, Mn). Solid State Commun. **337**, 114426 (2021)
Ciftci, Y.O., Mahanti, S.D.: Electronic structure and thermoelectric properties of half–Heusler compounds with eight electron valence count—KScX (X = C and Ge). J. Appl. Phys. **119**, 145703 (2016)
Crystalmaker software, crystalmaker, on-line URL http://www.crystalmaker.com.
Djelti, R., Besbes, A., Bestani, B.: TB-mBJ calculations of optical and thermoelectric properties of half-Heusler FeCrAs alloy. Opt. Quant. Electron. **52**, 414 (2020)
Djelti, R., Besbes, A., Bestani, B.: Investigation of electronic, optical and thermoelectric properties of new d^0 half-metallic half-Heusler alloys SiLiX (X=Ca and Sr). Emergent Mater. (2021). https://doi.org/10.1007/s42247-021-00256-9
Durukan, I.K., Ciftci, Y.O.: The effect of pressure on elastic anisotropy, vibration and optical properties of a AgScSi compound. J. Electron. Mater. **48**(6), 4050–4056 (2019)
Durukan, I.K., Ciftci, Y.O.: First-principles calculations of vibrational and optical properties of half- Heusler NaScSi. Indian J Phys **95**(11), 2303–2312 (2021)
Eliassen, S.N.H., Katre, A., Madsen, G.K.H., Persson, C., Løvvik, O.M., Berland, K.: Lattice thermal conductivity of $Ti_xZryHf_{1-x-y}NiSn$ half-Heusler alloys calculated from first principles: key role of nature of phonon modes. Phys. Rev. B **95**, 045202 (2017)
Forozani, Gh., Karami, F., Moradi, M.: Structural, electronic, magnetic, and optical properties of Ir_2ScZ (Z = Si, Ge, Sn) full-Heusler compounds: a first-principles study. J. Electron. Mater. **49**, 5947–5956 (2020)
Gajdoš, M., Hummer, K., Kresse, G., Furthmüller, J., Bechstedt, F.: Linear optical properties in the projector-augmented wave methodology. Phys. Rev. b. **73**, 045112 (2006)
Gueorguiev, G.K., Neidhardt, J., Stafström, S., Hultman, L.: First-principles calculations on the role of CN precursors for the formation of fullerene-like carbon nitride. Chem. Phys. Lett. **401**, 288 (2005)
Gupta, Y., Sinha, M.M., Verma, S.S.: Effect of pressure on dynamical stability, electronic and thermoelectric properties of equiatomic quaternary Heusler alloy LaCoTiGe. Mater. Sci. Semicond. Process. **141**, 106432 (2022)
Haines, J., Leger, J.M., Bocquillon, G.: Synthesis and design of superhard materials. Annu. Rev. Mater. Res. **31**, 1 (2001)
Hoat, D.M., Naseri, M.: Electronic and thermoelectric properties of RbYSn half-Heusler compound with 8 valence electrons: spin-orbit coupling effect. Chem. Phys. **528**, 110510 (2020)
Hoat, D.M., Naseri, M., Pérez, R.P., Rivas-Silva, J.F., Kartamyshev, A.I., Cocoletzi, G.H.: P-substitution effects on the electronic structure and thermal properties of the half-metallic half-Heusler NaCrBi compound. Chem. Phys. **537**, 110848 (2020)
Hohenberg, P., Kohn, W.: Inhomogeneous electron gas. Phys. Rev. **136**(3B), B864 (1964)
Hornstra, J., Bartels, W.: Determination of the lattice constant of epitaxial layers of III-V compounds. J. Cryst. Growth **44**, 513–517 (1978)
Hu, J.M., Huang, S.P., Xie, Z., Hu, H., Cheng, W.D.: First-principles study of the elastic and optical properties of the pseudocubic Si_3As_4, Ge_3As_4 and Sn_3As_4. J. Phys. Condens. Matter. **19**, 4962 (2007)
Huang, L., Zhang, Q., Yuan, B., Lai, X., Yan, X., Ren, Z.: Recent progress in half-Heusler thermoelectric materials. Mater. Res. Bull. **76**, 107–112 (2016)
Hussain, A., Kashif, M., Belabbas, M., Noreen, M., Janjua, F.R., Arbouche, O.: First principle calculation of mechanical stability, opto-electronic and thermo-electric properties of TaIrGe1-xSnx (0 x 1) Half-Heusler alloy. Comput. Conden. Matt. **25**, e00511 (2020)

Irfan, M., Kamran, M.A., Azam, S., Iqbal, M.W., Alharbi, T., Majid, A., Omran, S.B., Khenata, R., Bouhemadou, A., Wang, X.: Electronic structure and optical properties of TaNO: an ab initio study. J. Mol. Graph. Model. **92**, 296–302 (2019)

Jianga, Y., Na, L., Ma, H.: HPHT synthesis and enhanced thermoelectric transport properties of double-doped $Co_4Sb_{11}Te_xSn_{1-x}$ skutterudites. J. Alloy. Compd. **894**, 162426 (2022)

Kamlesh, P.K., Gautam, R., Kumari, S., Verma, A.S.: Investigation of inherent properties of XScZ (X = Li, Na, K; Z = C, Si, Ge) half-Heusler compounds: appropriate for photovoltaic and thermoelectric applications. Physica B **615**, 412536 (2021)

Kaur, K., Kumar, R., Rai, D.P.: A promising thermoelectric response of HfRhSb half Heusler compound at high temperature: a first principle study. J. Alloy. Compd. **763**, 1018–1023 (2018)

Khan, A.U., Kobayashi, K., Tanga, D.M., Yamauchia, Y., Hasegawa, K., Mitome, M., Xue, Y., Jiang, B., Tsuchiya, K., Golberg, D., Bando, Y., Mori, T.: Nano-micro-porous skutterudites with 100% enhancement in ZT for high performance thermoelectricity. Nano Energy **31**, 152–159 (2017)

Khandy, S.H., Chai, J.D.: Strain engineering of electronic structure, phonon, and thermoelectric properties of p-type half-Heusler semiconductor. J. Alloy. Compd. **850**, 156615 (2021)

Khandy, S.H., Kaur, K., Dhiman, S., Singh, J., Kumar, V.: Exploring thermoelectric properties and stability of half-Heusler PtXSn (X = Zr, Hf) semiconductors: a first principle investigation. Comput. Mater. Sci. **188**, 110232 (2021)

Kumar, V., Roy, D.R.: Structure, bonding, stability, electronic, thermodynamic and thermoelectric properties of six different phases of indium nitride. J. Mater. Sci. **53**, 8302–8313 (2018)

Madsen, G.K., Singh, D.J.: BoltzTraP. A code for calculating band-structure dependent quantities. Comput. Phys. Commun. **175**(1), 67 (2006)

Marius, G.: The Physics of Semiconductors: Kramers-Kronig Relations, pp. 775–776. Springer, Berlin Heidelberg (2010)

Monkhorst, H.J., Pack, J.D.: Special points for Brillouin-zone integrations. Phys. Rev. B **13**, 5188 (1976)

Nagura, J., Ashani, T.M., Adebambo, O.O., Ayedun, F., Adebayo, G.A.: Thermoelectric and mechanical properties of XHfSn (X=Ni, Pd and Pt) semiconducting Half-heusler alloys: a first-principles study. Comput. Condens. Matter. **26**, e00539 (2021)

Nourozi, B., Aminian, A., Fili, N., Zangeneh, Y., Boochani, A., Darabi, P.: The electronic and optical properties of MgO mono-layer: based on GGA-mBJ. Res. Phys. **12**, 2038–2043 (2019)

Parvin, F., Hossain, M.A., Ahmed, I., Akter, K., Islam, A.K.M.A.: First-principles calculations to investigate mechanical, optoelectronic and thermoelectric properties of half-Heusler p-type semiconductor BaAgP. Res. Phys. **23**, 104068 (2021)

Perdew, J.P., Burke, K., Ernzerhof, M.: Generalized gradient approximation made simple. Phys Rev Lett. **77**(18), 3865 (1996)

Poelman, D., Smet, P.F.: Methods for the determination of the optical constants of thin films from single transmission measurements: a critical review. J. Phys. D Appl. Phys. **36**, 1850 (2003)

Pugh, S.: Relations between the elastic moduli and the plastic properties of polycrystalline pure metals the London, Edinburgh, and Dublin. Philos. Mag. J. Sci. **45**, 823 (1954)

Rahman, A.U., Aurangzeb, M., Khan, R., Zhang, Q., Dahsha, A.: Predicted double perovskite material Ca_2ZrTiO_6 with enhanced n-type thermoelectric performance. J. Solid State Chem. **305**, 122661 (2022)

Rajendran, R.: John, First principles study on electronic properties and mechanical stability of HfRhZ (Z = As and Sb) half Heusler alloys. J. Cryst. Growth **581**, 126468 (2022)

Reshak, A.: Thermoelectric properties of the spin-polarized half-metallic ferromagnetic CsTe and RbSe compounds. RSC Adv. **6**, 98197–98207 (2016)

Rogl, G., Yubuta, K., Kerber, M., Grytsiv, A., Zehetbauer, M., Bauer, E., Rogl, P.: Sustainable and simple processing technique for n-type skutterudites with high ZT and their analysis. Acta Mater. **173**, 9–19 (2019)

Saini, S.M.: Structural, electronic and thermoelectric performance of narrow gap LuNiSb half Heusler compound: potential thermoelectric material. Physica B **610**, 412823 (2021)

Shakil, M., Masood, M.K., Zafar, M., Ahmad, S., Hussain, A., Gadhi, M.A., Buzdar, S.A., Iqbal, T.: Theoretical study of structural, electronic and optical properties of $In_xGa_{1-x}N$ alloys. Optik Int. J. Light Electron Opt. **174**, 739–747 (2018)

Shakil, M., Hassan, S., Arshad, H., Rizwan, M., Gillani, S.S.A., Rafique, M., Zafar, M., Ahmed, S.: Theoretical investigation of structural, magnetic and elastic properties of half Heusler LiCrZ (Z = P, As, Bi, Sb) alloys. Physica B **575**, 411677 (2019)

Shakil, M., Kousar, M., Gillani, S.S.A., Rizwan, M., Arshad, H., Rafique, M., Zafar, M.: First principle computation of half metallicity and mechanical properties of a new series of half Heusler alloys KMnZ (Z = B, Si, Ge, As) for spintronics. Indian J Phys **96**(1), 115–126 (2022)

Shang, H., Carbogno, C., Rinke, P., Scheffler, M.: Lattice dynamics calculations based on density-functional perturbation theory in real space. Comput. Phys. Commun. **215**, 26–46 (2017)
Singh, D.: Planes Waves, Pseudo-Potentials and the LAPW Method. Kluwer Academic Publishers, Boston, Dortrecht, London (1994)
Sun, J., Wang, H.T., Ming, N.B.: Optical properties of heterodiamond B_2CN using first-principles calculations. Appl. Phys. Lett. **84**, 4544 (2004)
Sun, H.L., Yang, C.L., Wang, M.S., Ma, X.G., Yi, Y.G.: High thermoelectric efficiency fluoride perovskite materials of $AgMF_3$ (M = Zn, Cd). Mater. Today Energy **19**, 100611 (2021)
Togo, A., Tanaka, I.: First principles phonon calculations in materials science. Scripta Mater. **108**, 1–5 (2015)
Tran, F., Blaha, P.: Accurate band gaps of semiconductors and insulators with a semilocal exchange-correlation potential. J. Phys. Rev. Lett. **102**, 226401 (2009)
Umamaheswari, R., Yogeswari, M., Kalpana, G.: Ab-initio investigation of half-metallic ferromagnetism in half-Heusler compounds XYZ(X=Li, Na, K and Rb; Y=Mg, Ca, Sr and Ba; Z=B, Al and Ga). J. Magn. Magn. Mater. **350**, 167–173 (2014)
Vasileska, D., Khan, H.R., Ahmed, S.S., Kannan, G., Ringhofer, C.: Quantum and Coulomb Effects in Nano Devices, Nano-Electronic Devices, pp. 97–181. Springer, Cham (2011)
Wang, S., Ye, H.: First-principles study on elastic properties and phase stability of III–V compounds. Phys. Status Solidi **240**, 45 (2003)
Wu, Z., Cohen, R.E.: More accurate generalized gradient approximation for solids. Phys. Rev. B **73**, 235116 (2006)
Zafar, M., Masood, M.K., Rizwan, M., Zia, A., Ahmad, S., Akram, A., Bao, C.C., Shakil, M.: Theoretical study of structural, electronic, optical and elastic properties of Al_xGa_{1-x} P. Optik Int. J. Light Electron Opt. **182**, 1176–1185 (2019)
Zhu, T., Fu, C., Xie, H., Liu, Y., Zhao, X.: High efficiency half-Heusler thermoelectric materials for energy harvesting. Adv. Energy Mater. **5**, 1500588 (2015)